Electronic Supplementary Material (ESI) for Dalton Transactions.
This journal is © The Royal Society of Chemistry 2024

Supporting Information

Electrocatalytic reduction of nitrite to ammonia on undercoordinated Cu

Ruichao Zhang *, Shiyao Shang, Fuzhou Wang, Ke Chu *

School of Materials Science and Engineering, Lanzhou Jiaotong University, Lanzhou 730070, China

*Corresponding authors. zhangrch11@163.com (R. C. Zhang), chuk630@mail.lzjtu.cn (K. Chu)

Experimental Section

Synthesis of u-Cu

Copper foam (CF, 1 cm × 1 cm) was immersed in the mixed solution of $(NH_4)_2S_2O_8$ (0.05 mol L^{-1}) and NaOH (1 mol L^{-1}) for 20 min. The obtained $Cu(OH)_2$ nanowires on CF was then annealed at 200 °C in H_2/Ar (v/v: 5/95) to acquire Cu nanowires. The dried Cu nanowires were further subjected to Ar plasma treatment for 5 min in an AX-1000 plasma system (13.56 MHz) to obtain undercoordinated Cu nanowires (u-Cu).

Electrochemical experiments

Electrochemical measurements were carried out using a CHI-760E electrochemical workstation employing a three-electrode cell system consisting of a u-Cu working electrode, an Ag/AgCl reference electrode and a Pt foil counter electrode. All the potentials were referenced to a reversible hydrogen electrode (RHE) by the following equation: E (V vs. RHE) = E (V vs. Ag/AgCl) + 0.198 V + 0.059 × pH. Electrochemical NO_2RR measurements were conducted in an H-type electrochemical cell containing 0.5 M Na_2SO_4 with 0.1 M $NaNO_2$ separated by Nafion 211 membrane. Both cathode chamber and anode chamber contain 35 mL of electrolyte. Prior to use, the Nafion membrane was pretreated by heating it in a 5% H_2O_2 aqueous solution at 80 °C for 1 h, followed by rinsing with deionized water at 80 °C for another 1 h. During the electrolysis, there is no agitation used. After each chronoamperometry test for 0.5 h electrolysis at a specific potential, the liquid products were analyzed using colorimetric methods with UV-vis absorbance spectrophotometer (MAPADA P5), while the gas products were analyzed using gas chromatography (Shimadzu GC2010).

Determination of NH_3

The NH_3 concentration in the electrolyte was determined using the an indophenol blue method[1]. Typically, 0.5 mL of electrolyte was extracted from the electrochemical reaction vessel and subsequently diluted tenfold with deionized water. Then 2 mL of diluted solution was removed into a clean vessel followed by sequentially adding NaOH solution (2 mL, 1 M) containing $C_7H_6O_3$ (5 wt.%) and $C_6H_5Na_3O_7$ (5 wt.%), NaClO (1 mL, 0.05 M), and $C_5FeN_6Na_2O$ (0.2 mL, 1wt.%)

aqueous solution. After incubation for 2 hours at room temperature. The mixed solution was measured in UV-Vis at 655 nm. The concentration-absorbance curves were calibrated using a range of concentrations in a standard NH_4Cl solution. Subsequently, the NH_3 yield rate and Faradaic efficiency (FE) were calculated using the following equation:

$$NH_3 \text{ yield rate} = (c \times V) / (17 \times t \times A) \quad (1)$$

Faradaic efficiency was calculated by the following equation:

$$FE = (6 \times F \times c \times V) / (17 \times Q) \times 100\% \quad (2)$$

where c (μg mL^{-1}) is the measured NH_3 concentration, V (mL) is the volume of electrolyte in the cathode chamber, t (s) is the electrolysis time and A is the surface area of CC (1×1 cm^2), F (96500 C mol^{-1}) is the Faraday constant, Q (C) is the total quantity of applied electricity.

Determination of N_2H_4

The N_2H_4 content in the electrolyte was quantitatively determined using the Watt and Chrisp method[2]. To prepare the coloring solution, a combination of 300 mL C_2H_5OH, 5.99 g $C_9H_{11}NO$, and 30 mL HCl was mixed. Subsequently, 5 mL of the coloring solution was introduced to 5 mL of the electrolyte. After the incubation for 20 min at room temperature, the mixed solution was subjected to UV-vis measurement using the absorbance at 455 nm wavelength. The concentration-absorbance curve is calibrated by a series of concentrations of standard N_2H_4 solutions.

Characterizations

X-ray diffraction (XRD) patterns were obtained using a Rigaku D/max 2400 diffractometer. Transmission electron microscopy (TEM) and high-resolution transmission electron microscopy (HRTEM) were acquired using a Tecnai G^2 F20 microscope. X-ray photoelectron spectroscopy (XPS) measurement was conducted on a PHI 5702 spectrometer.

Calculation details

Density functional theory (DFT) calculations were conducted using a Cambridge sequential total energy package (CASTEP). The method of the Perdew-Burke-

Ernzerhof (PBE) generalized gradient approximation (GGA) functional was utilized for the exchange-correlation potential. The DFT-D correction method was used to describe the van der Waals interactions. A cutoff energy of 450 eV was chosen and the 3×3×1 Monkhorst-Pack mesh was used in Brillouin zone sampling. Energy and force will not reach convergence until lower to 1.0×10^{-5} eV and 0.02 eV/Å, respectively. The In_1Cu (111) was modeled by a 4×4 supercell, and a vacuum region of 15 Å was used to separate adjacent slabs.

The computational hydrogen electrode (CHE) model was adopted to calculate the Gibbs free energy change (ΔG) for each elementary step as follows[3]:

$$\Delta G = \Delta E + \Delta E_{ZPE} - T\Delta S \tag{3}$$

where ΔE is the adsorption energy, ΔE_{ZPE} is the zero-point energy difference and $T\Delta S$ is the entropy difference between the gas phase and adsorbed state. The entropies of free gases were acquired from the NIST database.

MD simulations were performed using a force field type of Universal. The electrolyte system was modeled by a cubic cell with placing catalyst at the center of the cell and randomly filling 1000 H_2O, 50 NO_2^- molecules, and 50 H atoms. After geometry optimization, the MD simulations were performed in an NVT ensemble (298 K) with the total simulation time of 5 ns at a time step of 1 fs.

The radial distribution function (RDF) is calculated by[3]:

$$g(r) = \frac{dN}{4\pi\rho r^2 dr} \tag{4}$$

where dN is the amount of NO_2^- in the shell between the central particle r and $r+dr$, ρ is the number density of NO_2^-, H_2O, and H.

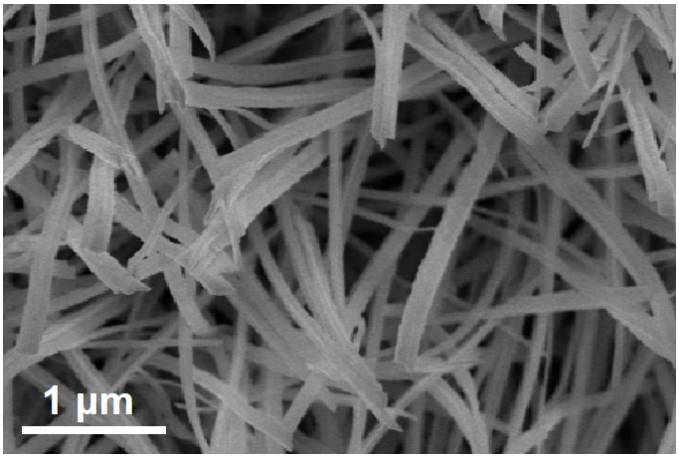

Fig. S1. SEM image of pristine Cu.

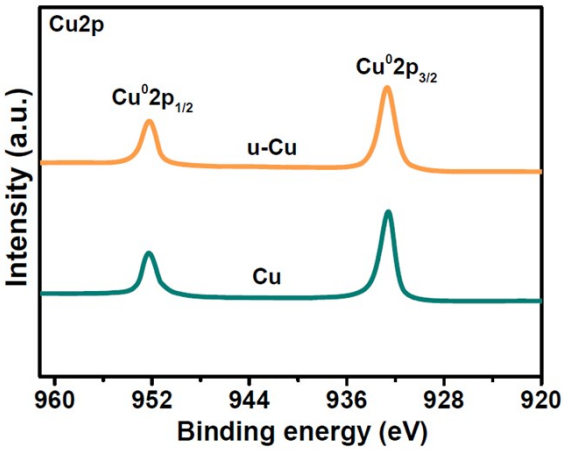

Fig. S2. XPS spectra of Cu and u-Cu.

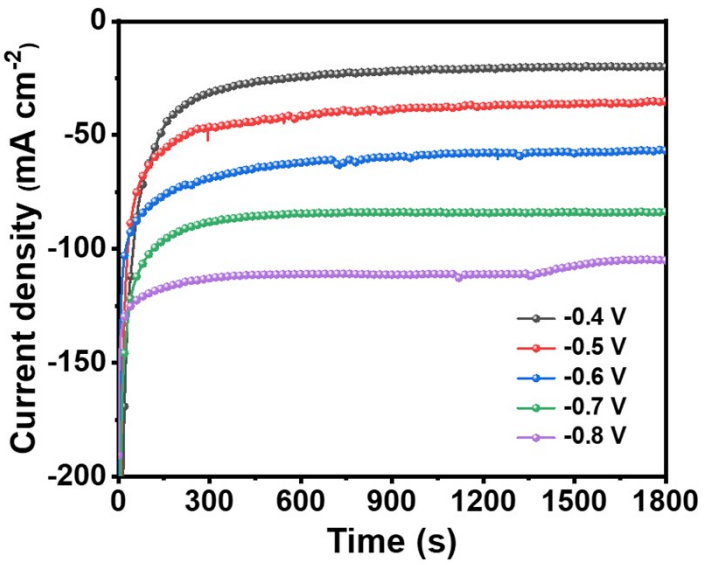

Fig. S3. Chronoamperometry test of u-Cu in 0.5 M Na_2SO_4 electrolyte with 0.1 M $NaNO_2$ at different potentials.

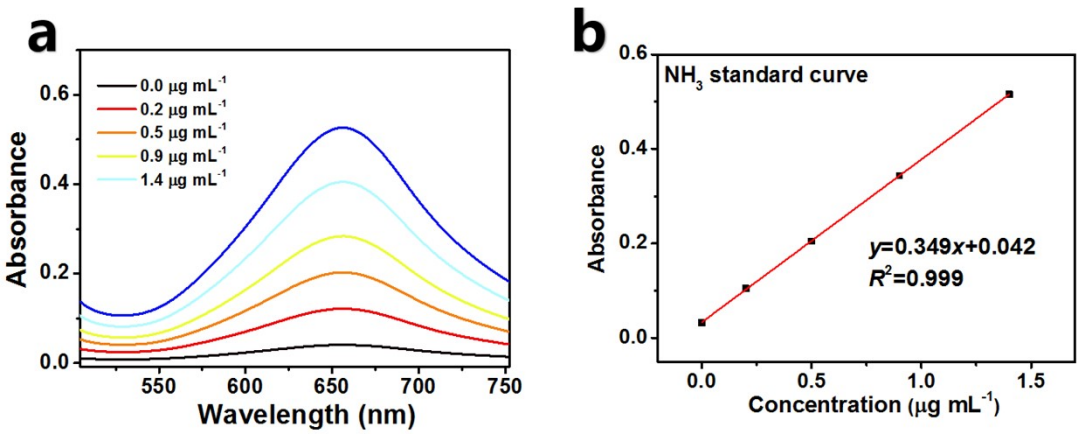

Fig. S4. (a) UV-vis absorption spectra of NH_4^+ assays after incubated for 2 h at ambient conditions. (b) Calibration curve used for the calculation of NH_3 concentrations.

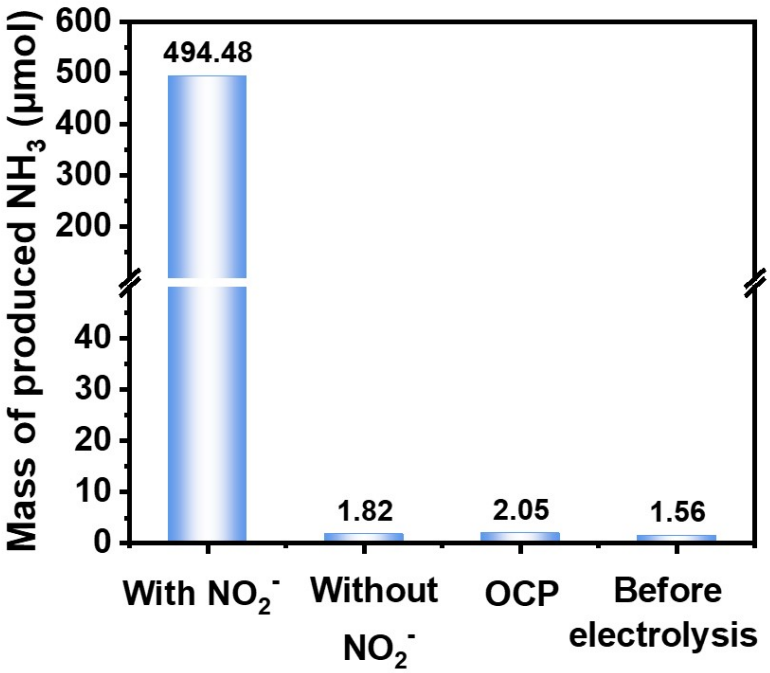

Fig. S5. Amounts of produced NH_3 on u-Cu under different conditions: (1) electrolysis in NO_2^--containing solution at -0.7 V vs. RHE, (2) electrolysis in NO_2^--free solution at -0.7 V vs. RHE, (3) electrolysis in NO_2^--containing solution at open-circuit potential (OCP), (4) before electrolysis.

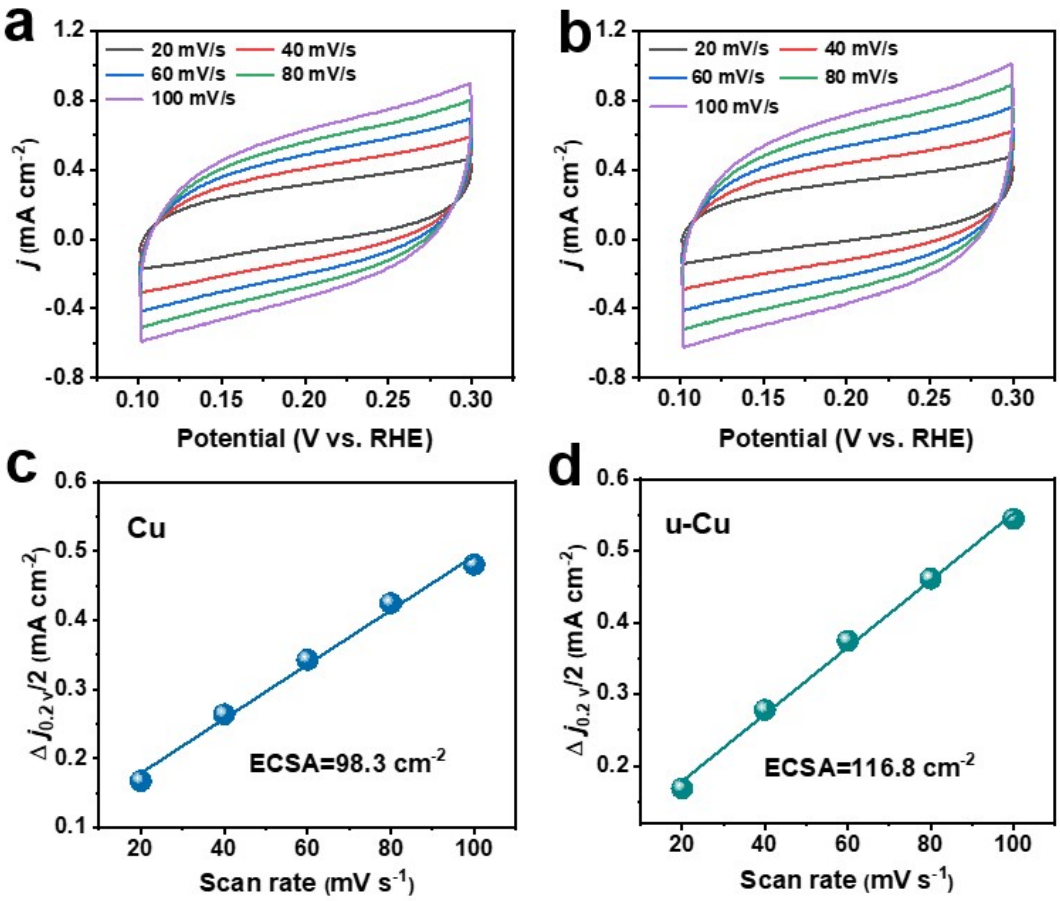

Fig. S6. CV measurements in 0.5 M Na_2SO_4 electrolyte with 0.5 M $NaNO_2$ at different scanning rates for (a, c) Cu and (b, d) u-Cu, and the corresponding calculated ECSA.

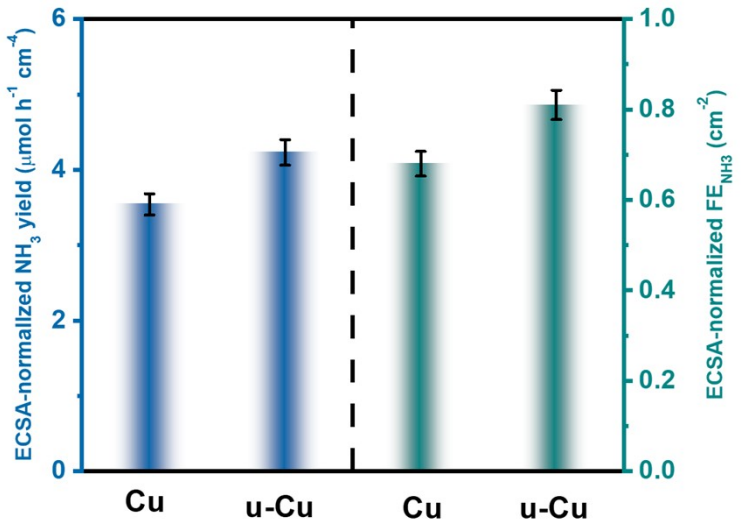

Fig. S7. Comparison of the ECSA-normalized NH_3 yield rates and FE_{NH3} between Cu and u-Cu at -0.7 V vs. RHE.

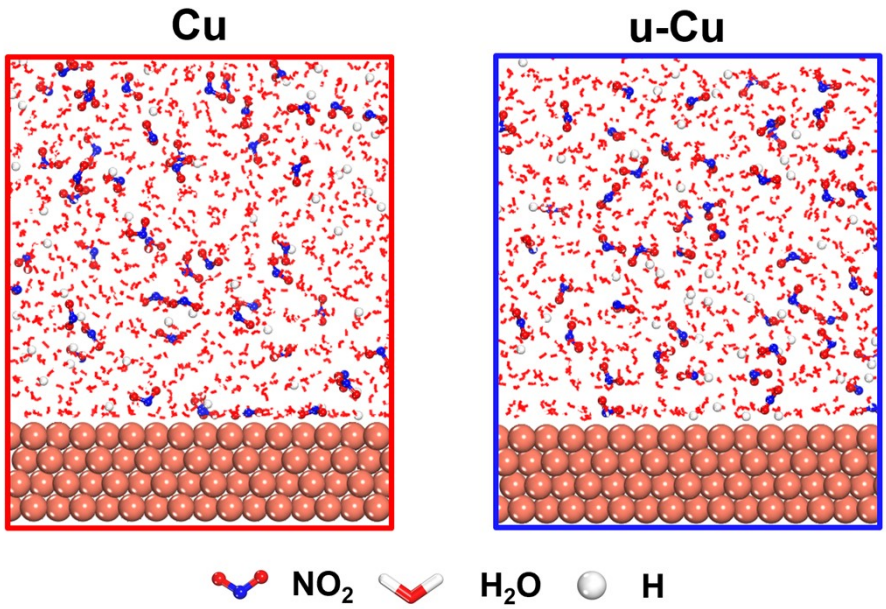

Fig. S8. Initial snapshots for the dynamic adsorption process of NO_2^- on Cu and u-Cu.

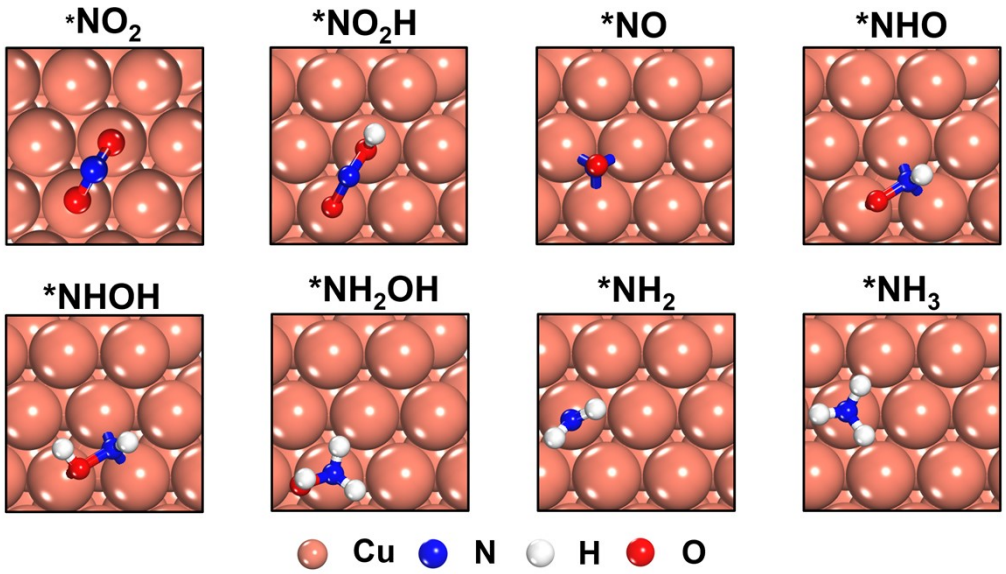

Fig. S9. Optimized atomic configurations of the NO_2RR reaction intermediates on Cu.

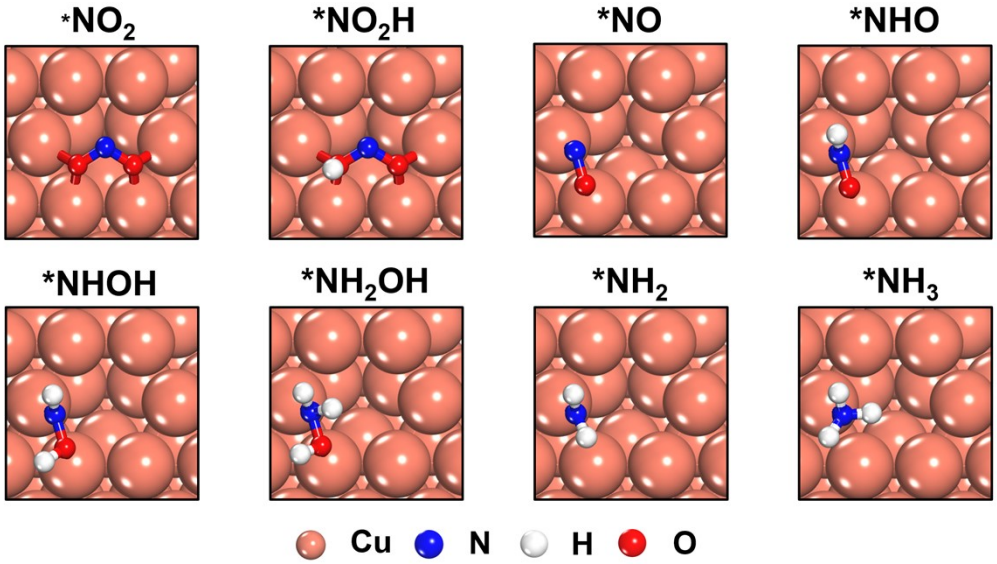

Fig. S10. Optimized atomic configurations of the NO_2RR reaction intermediates on u-Cu.

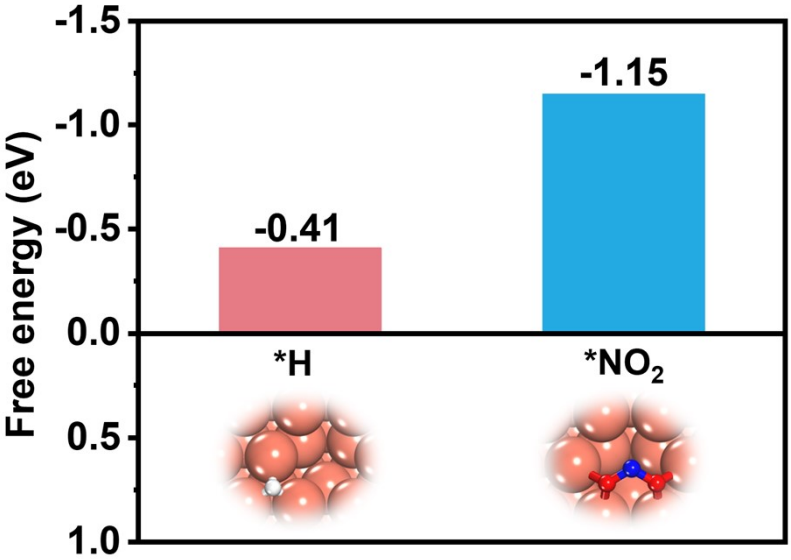

Fig. S11. Adsorption free energies of $*NO_2$ and *H on u-Cu.

Table S1. Comparison of the optimum NH_3 yield rate and NH_3-Faradic efficiency (FE_{NH3}) for the recently reported NO_2RR electrocatalysts at ambient conditions

Catalyst	Electrolyte	NH_3 yield rate (μ mol h^{-1} cm^{-2})	FE_{NH3}	Reference
P-TiO_2/TP	0.1 M Na_2SO_4 (0.1 M NO_2^-)	560.8	90.6%@-0.6 V	[4]
CoB@TiO_2/TP	0.1 M Na_2SO_4 (400 ppm NO_2^-)	233.1	95.2%@−0.7 V	[5]
Ag@NiO/CC	0.1 M NaOH (0.1 M NO_2^-)	338.3	96.1%@-0.7 V	[6]
Ni_2P/NF	0.1 M PBS (200 ppm NO_2^-)	191.3	90.2±3.0% @-0.3 V	[7]
CF@Cu_2O	0.1 M PBS (0.1 M NO_2^-)	441.8	94.2% @-0.6 V	[8]
V-TiO_2/TP	0.1 M NaOH (0.1 M NO_2^-)	540.8	93.2% @-0.6 V	[9]
CoP NA/TM	0.1 M PBS (500 ppm NO_2^-)	132.7±3.0	90±2.3% @-0.2 V	[10]
Cu_3PNA/CF	0.1 M PBS (0.1 M $NaNO_2$)	93.6	91.2±2.5% @-0.5 V	[11]
ITO@TiO_2/TP	0.5 M $LiClO_4$ (0.1 M NO_2^-)	411.3	82.6% @-0.5 V	[12]
u-Cu	**0.5 M Na_2SO_4 (0.1 M NO_2^-)**	**494.5**	**94.7% @-0.7 V**	**This work**

References

[1] D. Zhu, L. Zhang, R.E. Ruther, R.J. Hamers, Nat. Mater. 12(9) (2013) 836-841.

[2] G.W. Watt, J.D. Chrisp, Anal. Chem. 24(12) (1952) 2006-2008.

[3] X. Li, P. Shen, Y. Luo, Y. Li, Y. Guo, H. Zhang, K. Chu, Angew. Chem. Int. Edit. 134 (2022) e202205923.

[4] L. Ouyang, X. He, S. Sun, Y. Luo, D. Zheng, J. Chen, Y. Li, Y. Lin, Q. Liu, A.M. Asiri, X. Sun, J. Mater. Chem. A 10(44) (2022) 23494-23498.

[5] L. Hu, D. Zhao, C. Liu, Y. Liang, D. Zheng, S. Sun, Q. Li, Q. Liu, Y. Luo, Y. Liao, L. Xie, X. Sun, Inorg. Chem. Front. 9(23) (2022) 6075-6079.

[6] Q. Liu, G. Wen, D. Zhao, L. Xie, S. Sun, L. Zhang, Y. Luo, A. Ali Alshehri, M.S. Hamdy, Q. Kong, X. Sun, J. Colloid Interface Sci. 623 (2022) 513-519.

[7] G. Wen, J. Liang, L. Zhang, T. Li, Q. Liu, X. An, X. Shi, Y. Liu, S. Gao, A.M. Asiri, Y. Luo, Q. Kong, X. Sun, J. Colloid Interface Sci. 606 (2022) 1055-1063.

[8] Q. Chen, X. An, Q. Liu, X. Wu, L. Xie, J. Zhang, W. Yao, M.S. Hamdy, Q. Kong, X. Sun, Chem. Commun. 58(4) (2022) 517-520.

[9] H. Wang, F. Zhang, M. Jin, D. Zhao, X. Fan, Z. Li, Y. Luo, D. Zheng, T. Li, Y. Wang, B. Ying, S. Sun, Q. Liu, X. Liu, X. Sun, Mater. Today Phys. 30 (2023) 100944.

[10] G. Wen, J. Liang, Q. Liu, T. Li, X. An, F. Zhang, A.A. Alshehri, K.A. Alzahrani, Y. Luo, Q. Kong,

X. Sun, Nano Res. 15(2) (2022) 972-977.
[11] J. Liang, B. Deng, Q. Liu, G. Wen, Q. Liu, T. Li, Y. Luo, A.A. Alshehri, K.A. Alzahrani, D. Ma, X. Sun, Green Chem. 23(15) (2021) 5487-5493.
[12] S. Li, J. Liang, P. Wei, Q. Liu, L. Xie, Y. Luo, X. Sun, eScience 2(4) (2022) 382-388.